RSC Advances

PAPER

View Article Online
View Journal | View Issue

Cite this: *RSC Adv.*, 2024, **14**, 1977

Catalytic fabrication of graphene, carbon spheres, and carbon nanotubes from plastic waste

Eslam Salama, *[a] Safaa Mohamed,[a] Mahmoud Samy,[b] Kenneth Mensah, [c] Mona Ossman,[a] Marwa F. Elkady[de] and Hassan Shokry Hassan[fg]

In this study, we reported sustainable and economical upcycling methods for utilizing plastics such as polyethylene terephthalate (PET) and polypropylene (PP) compiled from the garbage of a residential area as cheap precursors for the production of high-value carbon materials such as graphene (G), carbon spheres (CS), and carbon nanotubes (CNTs) using different thermal treatment techniques. Graphene, carbon spheres, and carbon nanotubes were successfully synthesized from PET, PP, and PET, respectively *via* catalytic pyrolysis. XRD and FTIR analyses were conducted on the three materials, confirming the formation of carbon and their graphitic structure. TEM images displayed uniform and consistent morphological structures of the fabricated materials. EDX data confirmed that the prepared carbon-based materials only contained carbon and oxygen without any significant contaminations. XPS results revealed significant peaks in the C 1s spectra associated with sp^2 and sp^3 hybridized carbon for the three materials. BET spectra showed that the prepared CNTs (54.872 m^2 g^{-1}) have the highest surface area followed by carbon spheres (54.807 m^2 g^{-1}). The thermal stability of graphene surpassed both carbon spheres and carbon nanotubes which is mainly attributed to the stronger inter-molecular bonds of graphene. Based on the characterization of the prepared materials, these materials are promising to be utilized in environmental remediation applications due to their high carbon content, low cost, and high surface area.

Received 29th October 2023
Accepted 4th January 2024

DOI: 10.1039/d3ra07370j

rsc.li/rsc-advances

1. Introduction

The yearly massive production of plastics and the improper management of these plastics have received global concern owing to the adverse environmental impacts related to the presence of plastics in the environment.[1] Plastics are stable and can remain in the environment for hundreds of years without degradation.[2] Due to the low density of plastic waste, it can transfer to water streams and sometimes people dispose of plastic waste directly in water sources as one of the unsuitable management approaches.[3] The presence of plastics in water streams can harm aquatic organisms and may lead to their death.[4] Landfills and incinerators are another improper management method of plastic waste. Around 79% of plastic waste is dumped into landfills which could result in the leaching of plastics into the soil and groundwater.[5] Therefore, plants can adsorb plastics which can result in the transfer of these plastics to humans *via* the food chain.[5] Additionally, plastics' surfaces can carry toxic contaminants.[6] On the other hand, managing plastic wastes by incineration can result in the pollution of air and the increase of greenhouse gas emissions.[7] Accordingly, it is imperative to develop an effective management approach for plastic waste that overcomes the problems associated with traditional management techniques.

The utilization of plastic waste as a precursor for the synthesis of value-added products (*e.g.*, carbonaceous materials) has magnetized great solicitude as a sustainable management approach. Plastic wastes contain high carbon content with limited inorganic impurities which qualify them to be used as a precursor for the production of carbon rich materials.[8] Different carbonaceous materials can be prepared from plastic waste such as graphene,[9] activated carbon[10] and carbon nanotubes.[11] The conversion of plastics to the

[a]*Environment and Natural Materials Research Institute (ENMRI), City of Scientific Research and Technological Applications (SRTA-City), New Borg El-Arab City, Alexandria 21934, Egypt. E-mail: esalama@srtacity.sci.eg*

[b]*Department of Public Works Engineering, Faculty of Engineering, Mansoura University, Mansoura 35516, Egypt*

[c]*Department of Civil and Environmental Engineering, University of Maine, Orono, ME 04469, USA*

[d]*Fabrication Technology Research Department, Advanced Technology and New Materials Research Institute (ATNMRI), City of Scientific Research and Technological Applications (SRTA-City), New Borg El-Arab City, Alexandria 21934, Egypt*

[e]*Chemical and Petrochemical Engineering Department, Egypt-Japan University of Science and Technology (E-JUST), New Borg El-Arab City, Alexandria 21934, Egypt*

[f]*Electronic Materials Research Department, Advanced Technology and New Materials Research Institute (ATNMRI), City of Scientific Research and Technological Applications (SRTA-City), New Borg El-Arab City, Alexandria 21934, Egypt*

[g]*Environmental Engineering Department, Egypt-Japan University of Science and Technology, New Borg El-Arab City, Alexandria 21934, Egypt*

aforementioned valuable materials can contribute to the sustainable management of plastic wastes leading to the control of the environmental hazards related to plastics and reducing the reliance on landfilling and incineration for managing plastics. The produced carbonaceous materials are inexpensive because of the abundance of plastic waste, and they can be produced on a large-scale. Therefore, the produced carbon-rich materials can be employed in various environmental remediation technologies such as adsorption,[12] persulfate activation,[13] periodate activation,[14] photocatalysis[15] and Fenton[16] techniques. The utilization of carbonaceous materials prepared from plastic waste in the aforementioned treatment systems can reduce the treatment cost and facilitate the full-scale of these techniques.

In this study, mineral water plastic bottles, plastic drinking cups, and plastic yogurt cups were utilized as precursors for the preparation of carbon-rich materials such as graphene, carbon spheres and carbon nanotubes. The chemical composition, chemical structure, functional groups and morphology of the prepared materials were investigated using energy dispersive X-ray spectroscopy, X-ray diffraction, Fourier transform infrared spectroscopy and transmission electron microscopy, respectively. Further, chemical states and thermal stability of the prepared materials were studied by X-ray photoelectron spectroscopy and thermogravimetric analysis. Moreover, the surface area of the synthesized materials was estimated using BET surface area analyzer.

2. Experimental

2.1 Materials

Post-consumer waste plastic bottles, plastic drinking cups, and plastic yogurt cups were obtained from the garbage of a residential area in Alexandria, Egypt. All the gathered plastics were washed, shredded, and dried at room temperature prior their usage in the preparation process. Iron chloride anhydrous ($FeCl_3$, MW = 162.21), citric acid anhydrous crystalline ($C_6H_8O_7$, MW = 192.13), and nickel chloride hexahydrate ($NiCl_2 \cdot 2H_2O$, MW = 237.71) were purchased from Fisher Bio-Reagents, USA. Aluminum nitrate nonahydrate ($Al(NO_3)_3 \cdot 9H_2O$, ASC reagent 98%, MW = 375.13) and Hydrofluoric acid [HF] (48 wt% in H_2O, ≥99.99%) were purchased from Sigma Aldrich, USA. Stöber silica spheres were obtained from Sharc Matter, UK.

2.2 Synthesis of graphene from plastic waste

Catalytic pyrolysis is a promising method to fabricate high-value carbon materials while reducing oxygenated compounds, lowering viscosity, and increasing stability.[17] Firstly, a catalyst was prepared by citric acid combustion method, where 8.11 g $FeCl_3$, 18.756 g $Al(NO_3)_3 \cdot 9H_2O$, and 9.606 g citric acid were mixed at an equal molar ratio. The mixture was kept on continuous stirring on a hotplate at 120 °C until a viscous orange gel was obtained. Then, the gel was dried at 90 °C overnight. Next, the powder was calcined in a muffle furnace at 350 °C for 3 h. Finally, the catalyst was grounded into a fine powder.

5 g of the prepared catalyst was added to 10 g of the washed and shredded polyethylene terephthalate (PET) = plastic cups inside a stainless-steel reactor. Then, the reactor was placed in a muffle furnace at 800 °C for 2 h in the presence of nitrogen flow as shown in Fig. 1a.[18] The produced black char was grinned using a mortar for further characterization.

2.3 Synthesis of carbon spheres (CS) from plastic waste

In order to fabricate carbon spheres, 4 g of the washed and shredded polypropylene (PP) yogurt cups contained in a quartz boat was placed in the first stage of a tube-furnace reactor (NABERTHERM R 120/500/13 Compact tube furnace) and 2 gm of Stöber silica spheres (performs as a catalyst) was placed in the middle of the second stage of the tube-furnace reactor as shown in Fig. 1b. The temperature of the second stage reactor was elevated from room temperature to 900 °C with an increase rate of 10 °C min^{-1} under a flow of nitrogen.

Once the temperature of the catalyst stage reached 900 °C, the temperature of the pyrolysis stage of the furnace was ramped up to 500 °C at a ramping rate of 10 °C min^{-1}. Polypropylene gas flow generated from the pyrolysis of PP waste flushed the Stöber spheres' surface for 1 h. After, the tube furnace was allowed to cool to room temperature. The yield of this process is silica/carbon material. Carbon spheres were obtained by removing the Stöber silica template, using 10 mL of 10% HF solution for 24 h.[19] Finally, carbon spheres were carefully filtered and washed with distilled water several times until a neutral pH of the water was reached.

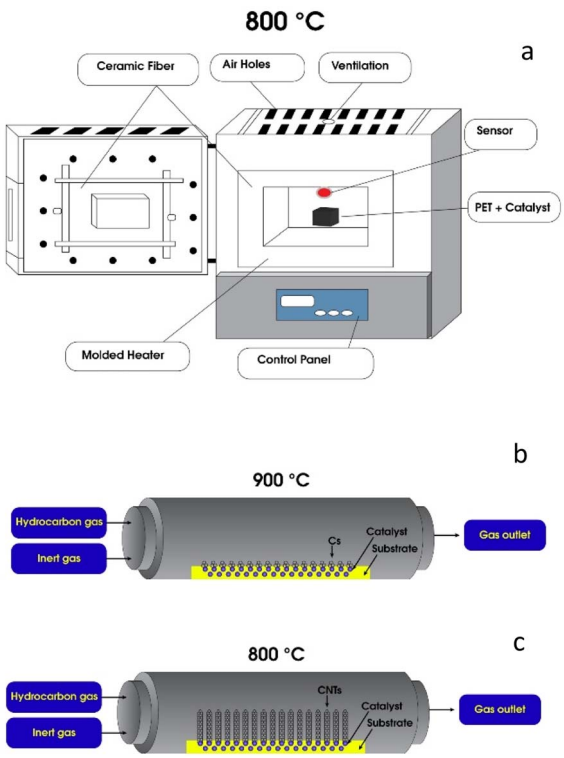

Fig. 1 Schematic illustration of catalytic fabrication of graphene (a), synthesis of carbon spheres (b), and fabrication carbon nanotubes (c).

2.4 Synthesis of carbon nanotubes (CNTs) from plastic waste

A metal-based catalyst was prepared by the wet-impregnation method, where nickel and iron were employed as the base metals as shown in Fig. 1c. Nickel-based catalysts have been shown to improve the efficiency of the pyrolysis process, as higher amounts of hydrogen are produced.[20] Ni to Fe molar ratio of 1 : 3 was selected based on the previous studies.[21–23] 13.68 g of $NiCl_2 \cdot 6H_2O$ and 24.33 g of $FeCl_3$ were firstly dissolved in ethanol and then placed on a hotplate at 50 °C under a continuous stirring, followed by the addition of a support material (metal loading) until 10 wt% was achieved. The mixture was stirred for 4 h and dried at 100 °C in an oven overnight. Afterward, the dry catalyst powder was calcined at 800 °C in a muffle for 3 h in air with a heating rate of 10 °C min^{-1}.[11] 4 g of the washed and shredded PET plastic bottles were thermally treated using a catalytic pyrolysis tube-furnace.[24–26] The sample was placed in a quartz boat in the first stage of the tube-furnace. 2 g of the catalyst was placed in a quartz boat in the second stage, where the catalysis temperature was set to 800 °C. Carrier gas (nitrogen) was supplied at a flow rate of 100 mL min^{-1}. Once the catalyst achieved the desired temperature, the plastic sample was heated to 500 °C with an increase rate of 30 °C min^{-1}. The final pyrolysis temperature was held for 20 min and then the furnace was allowed to cool.

2.5 Characterization of the produced carbon-based materials

Graphene, carbon spheres, and carbon nanotubes were characterized using different techniques such as: Fourier transform infrared analysis (FTIR) (Bruker Bremen, Germany), X-ray diffraction (XRD) using an X-ray powder diffractometer (CuK α1 radiation, $\lambda = 1.54056$ Å) at 40 kV and 40 mA and intensity data for 2θ from 20° to 80° over a period of 30 min (Schimadzu-7000, Shimadzu Corporation, Kyoto, Japan), transmission electron microscope (TEM) and energy dispersive X-ray spectroscopy (EDX) (JEOL, JEM-2100, Japan with an accelerating voltage of 80 kV), X-ray photoelectron spectroscopy (XPS) (Thermo Fisher Scientific, USA), Brunauer–Emmett–Teller (BET) surface area analyzer (Beckman Coulter SA3100, Brea, CA, USA), and the measurement of the N_2 adsorption–desorption isotherms were performed at 77 K. All samples were degassed before measurements under vacuum at room temperature for 12 h, and finally thermogravimetric analysis (TGA) (Shimadzu TGA-50 instrument).

3. Results and discussion

3.1 Morphological structure of the synthesized carbon materials

The morphological structure of the synthesized carbon materials was determined using TEM. TEM images confirm that the carbon structure in the case of the graphene is likely to be in form of a single, or a few layers sheet as indicated in Fig. 1a. The surface morphology and porosity of carbon spheres grow in a specific manner at elevated temperatures during the pyrolysis process. In these polycondensation reactions, carbon-containing materials can form an extended polymer chain that can curl up around a center point to form carbon spheres if suitable conditions are achieved.[27] Fig. 2a shows the TEM analysis of graphene, the outline of graphene flakes can be detected among the stalked graphene layers. The average diameter of the graphene flake is around 3.2 nm. Fig. 2b illustrates the formation of carbon spheres with a well-defined spherical structure having an average diameter of 32 nm. As shown in Fig. 2c, the structure of carbon nanotubes is clearly observed. They are homogeneous, with a diameter that ranges from 5 to 12 nm, which is well visible in TEM images. The results also confirm that the carbon nanotubes synthesized by this method showed poor crystallinity resulting from the dispersed graphene sheath that is not properly aligned and present in a disordered form.[28]

3.2 Chemical properties of prepared carbon materials

The chemical structures and crystallinity of graphene, carbon spheres, and carbon nanotubes were investigated *via* XRD as depicted in Fig. 3. Both graphene and carbon spheres have diffraction peaks at around $2\theta = 25$–26° which can be indexed to (002) crystal plane of graphitic structures[29] and another smaller peak at around $2\theta = 43°$ that is attributed to the (100) diffraction plane of graphitic structures. The weak peaks around 23.2° and 42.1° for (002) and (101) planes, respectively were observed indicates the absence of high regularity stacked graphene structure confirming the results of TEM analysis. On the other hand, XRD analysis of carbon nanotubes indicates a different pattern. A sharp and intense peak at 29.4° corresponds to the (002) reflection plane which affirms that a tetragonal arrangement of carbon atoms is formed[30] indicating that a high level of crystalline carbon structure is obtained.[31,32] Despite the sharp peak at the (002) plane, the resulting carbon-based material can be non-crystalline with a periodic structure that results in a distinct X-ray diffraction peak. This phenomenon can be due to the production of some extra hexagonal peak arrays which can be noticed multiple times at different azimuths but at much

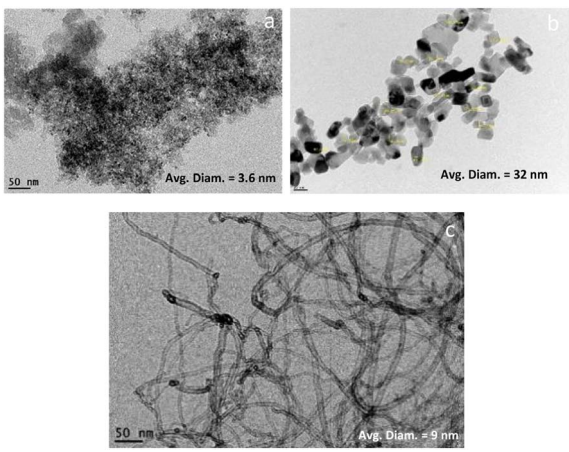

Fig. 2 TEM images of graphene (a), carbon spheres (b), and carbon nanotubes (c).

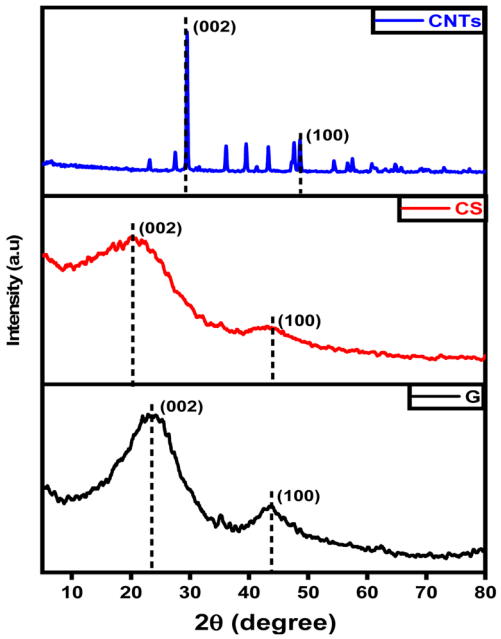

Fig. 3 XRD patterns of graphene, carbon spheres, and carbon nanotubes.

lower intensity compared to the main graphitic peak as a result of the passage of X-ray beams through the empty central core of a small tube.[20] The XRD pattern of the CNTs also shows that nickel, nickel oxide, and iron oxide were present in the spectrum attributable to the catalyst used. In a high-temperature environment (above 400 °C), nickel and iron react with oxygen and become nickel/iron oxide. The typical peaks near 43.2° and 53.74° disappeared due to existing Ni and Fe.[13,33,34]

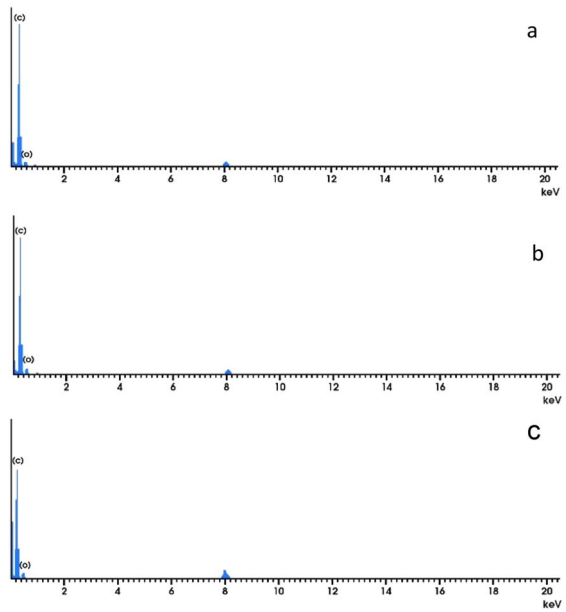

Fig. 4 EDX analysis of graphene (a), carbon spheres (b), and carbon nanotubes (c).

EDX spectroscopy specified the elemental composition of materials as shown in Fig. 4. It was observed that only high-intensity carbon and low content of oxygen are detected corresponding to (002) and (100) planes and there are no other visible peaks indicating that the material is free of contamination.

Table 1 presents the structural carbon/oxygen content which provides an excellent platform for both the chemical composition and morphology of the materials.[35] As shown in Table 1, graphene possesses the highest carbon content compared to carbon spheres and carbon nanotubes which suggests a stacked array of graphene layers. The higher oxygen content in both carbon spheres and carbon nanotubes may be attributed to the amorphous nature of the material.

The functional groups of the fabricated graphene, carbon spheres, and carbon nanotubes were specified using FTIR as shown in Fig. 5. The three products contain distinctive O–H stretching vibrations around the 3400 cm^{-1} range.[36,37] This bond is associated with the presence of amorphous carbon.[12,13,38–40] The smaller peaks at 2800 cm^{-1} to 2900 cm^{-1} correspond to the stretching vibration of the C–H bond.[41–43] Further, a stretching vibration of C=C=O can be noticed around 2300 cm^{-1}. The peaks at around 1600 cm^{-1} are due to the stretching vibration of carboxyl groups C=O.[44–47] The three products own the same main functional groups due to their carbonic structures.

The chemical composition and chemical states of the synthesized carbon materials were analyzed using XPS. Fig. 6 shows the high-resolution survey, C 1s, and O 1s spectra of the different structures. The C 1s spectrum of graphene is characterized by the peaks at 284.62 ± 0.1, 286.27 ± 0.1, and 288.38 ± 0.2 eV, which are imputed to the C=C (sp^2 bonded carbons), C–C (sp^3 bonded carbons), and carbonyl C=O.[48] On the other hand, the peaks in carbon spheres at 284.38 ± 0.1, 285.96 ± 0.1, 286.77 ± 0.1, and 288.3 ± 0.2 eV correspond to the C=C (sp^2 bonded carbons), C–C (sp^3 bonded carbons), alkoxy C–O–H and carbonyl C=O, while carbon nanotubes had peaked at 284.83 ± 0.1 eV, 286.18 ± 0.1 eV, 288.14 ± 0.1 eV and 289.7 ± 0.1 eV which are associated with sp^2 and sp^3 hybridized carbon (C=C and C–C), hydroxyl/phenols (C–OH) and carboxyl (O–C=O) groups, respectively.[49–51]

3.3 Physical characteristics of the fabricated carbon materials

The thermal behavior of graphene, carbon spheres, and carbon nanotubes was examined by thermal gravimetric analysis (TGA)

Table 1 Elemental content of graphene, carbon spheres, and carbon nanotubes

	Element content wt%	
Sample	C	O
Graphene	97.98	2.02
Carbon spheres	96.59	3.41
Carbon nanotubes	95.51	4.49

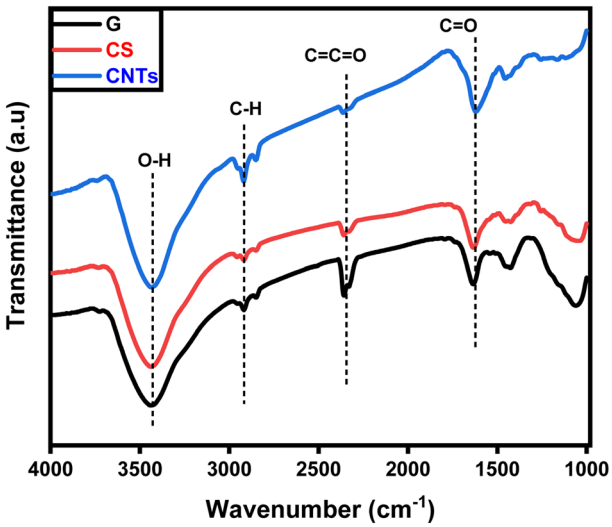

Fig. 5 FTIR analysis of graphene, carbon spheres, and carbon nanotubes.

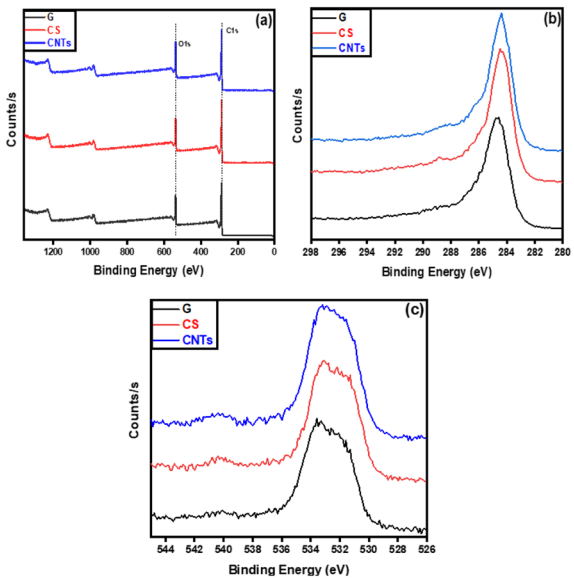

Fig. 6 XPS analysis of graphene (G), carbon spheres (CS), and carbon nanotubes (CNTs); XPS survey of G, CS, and CNTs (a), C 1s spectra of G, CS, and CNTs (b), and O 1s spectra of G, CS, and CNTs (c).

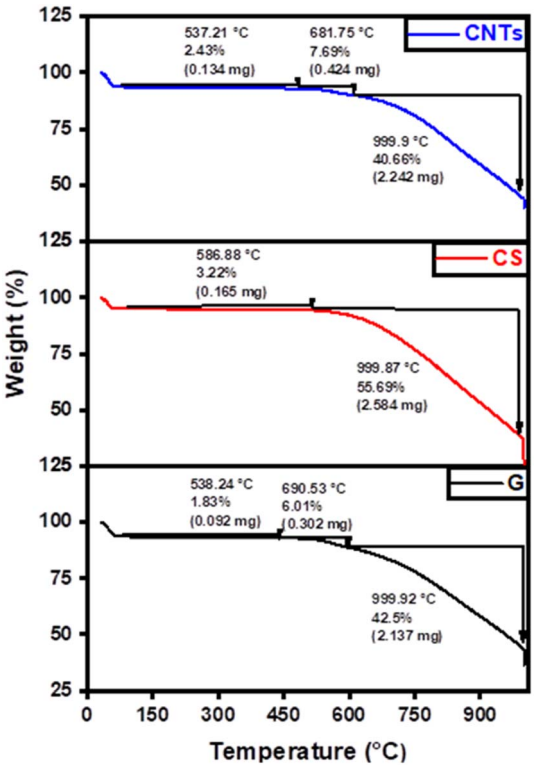

Fig. 7 TGA analysis of graphene (G), carbon spheres (CS), and carbon nanotubes (CNTs).

in a nitrogen atmosphere, to identify the quality of their thermal characteristics and possible structural deterioration. The TGA behavior is mainly affected by the number of layers, particle size, defects, and oxygen level.[52] As shown in Fig. 7, graphene started to lose weight at 32 °C, which is related to the physically adsorbed moisture, whereas the sudden weight loss at 650 °C is attributed to the combustion of the carbon backbone to carbon dioxide. The results affirmed that graphene had the highest thermal stability, where mass loss ratios of 50.34%, 50.78%, and 58.91% were achieved in the case of graphene, carbon nanotubes, and carbon spheres, respectively due to the removal of moisture and the decomposition carbon backbone. On the other hand, the mass loss ratio in the case of carbon spheres was around 3.22% compared to 10.12% in the case of carbon nanotubes until 690 °C which affirmed the high thermal stability of carbon spheres under low temperature and the high thermal stability of carbon nanotubes under higher temperatures.

To further investigate the structural morphology and its influence on physical properties, nitrogen physisorption measurements were conducted to investigate the surface area and porosity of the samples using BET analyzer as shown in Fig. 8. The nitrogen adsorption–desorption curves of graphene exhibited a typical type IV isotherm, suggesting a porous structure of the composite. The BET-specific surface area of the fabricated graphene was 11.860 $m^2\ g^{-1}$ with an average pore diameter of 9.518 nm. A large hysteresis area is observed, indicative of a wide distribution of pore sizes. The adsorption–desorption curves of the carbon spheres and carbon nanotubes showed a greater pore diameter compared to graphene (14.454 nm and 15.557 nm, respectively) despite having the same chemical graphitic composition, they showed distinctly different physical properties. The surface area and pore diameter of carbon nanotubes are mainly affected by the number of walls, tube diameter, and impurities.[47,53–55] The reported values for the surface area of single-walled CNTs ranged from ~150 $m^2\ g^{-1}$ to 600 $m^2\ g^{-1}$, and from ~15 $m^2\ g^{-1}$ to 300 $m^2\ g^{-1}$ for multi-walled CNTs.[56] The total pore volume of graphene, carbon spheres, and carbon nanotubes are 2.823 $cm^3\ g^{-1}$, 0.183 $cm^3\ g^{-1}$, and 0.214 $cm^3\ g^{-1}$, respectively.

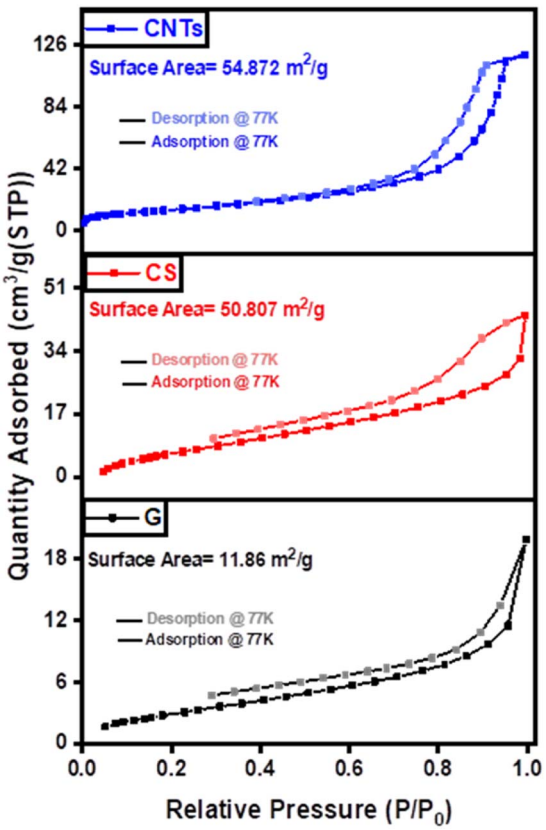

Fig. 8 Adsorption–desorption curves of graphene (G), carbon spheres (CS), and carbon nanotubes (CNTs).

4. Conclusions

Three carbon-derived materials were successfully synthesized using catalytic pyrolysis technique utilizing different common plastic wastes (plastic cups, yogurt cups, and plastic bottles). XRD, FTIR, and EDX results of the three materials confirmed the formation of carbon and its graphitic structure and the presence of the main active surface groups associated with graphene, carbon spheres, and carbon nanotubes as well as the chemical composition. The presence of sp^2 and sp^3 hybridized carbon in the C 1s spectra reaffirmed the chemical structure of the three materials. CNTs exhibited the highest surface area of 54.872 m^2 g^{-1} compared to graphene and carbon spheres. Graphene showed the highest thermal stability attaining a mass loss ratio of 50.34% followed by CNTs and carbon spheres. TEM images revealed a smooth and uniform morphology for the three materials. This study presents promising carbonaceous materials that can be used in various environmental purification applications such as adsorption, persulfate activation, and periodic activation processes due to their cheapness and high carbon ratios.

Author contributions

ES: conceptualization, methodology, investigation, writing – original draft, writing – review & editing. SM & MS & KM: writing – original draft, conceptualization, methodology. MO & ME & HS: validation, formal analysis, visualization, writing – review & editing, supervision, resources, funding acquisition.

Conflicts of interest

There are no conflicts of interest to declare.

Acknowledgements

This paper is based upon work supported by Science, Technology & Innovation Funding Authority (STDF) under a grant (46138).

Notes and references

1 M. C. Ariza-Tarazona, J. F. Villarreal-Chiu, J. M. Hernández-López, J. R. De la Rosa, V. Barbieri, C. Siligardi and E. I. Cedillo-González, *J. Hazard. Mater.*, 2020, **395**, 122632.
2 R. Geyer, J. R. Jambeck and K. L. Law, *Sci. Adv.*, 2017, **3**, e1700782.
3 P. Jiang, S. Zhao, L. Zhu and D. Li, *Sci. Total Environ.*, 2018, **624**, 48–54.
4 M. C. Ariza-Tarazona, J. F. Villarreal-Chiu, V. Barbieri, C. Siligardi and E. I. Cedillo-González, *Ceram. Int.*, 2019, **45**, 9618–9624.
5 M. A. Malla, A. Dubey, A. Kumar and S. Yadav, *Process Saf. Environ. Prot.*, 2023, **170**, 372–379.
6 S. Tang, L. Lin, X. Wang, A. Feng and A. Yu, *J. Hazard. Mater.*, 2020, **386**, 121960.
7 M. Samy, M. G. Alalm, M. N. Khalil, E. Ezeldean, A. El-Dissouky, M. Nasr and A. Tawfik, *J. Environ. Manage.*, 2023, **332**, 117402.
8 K. Mensah, H. Mahmoud, M. Fujii and H. Shokry, *J. Water Process. Eng.*, 2022, **45**, 102512.
9 S. Pandey, A. Kumar, M. Karakoti, K. K. Garg, A. Rana, G. Tatrari, B. S. Bohra, P. Yadav, R. K. Singh and N. G. Sahoo, *Nanoscale Adv.*, 2021, **3**, 4726–4738.
10 M. Kumari, G. R. Chaudhary, S. Chaudhary and A. Umar, *Chemosphere*, 2022, **294**, 133692.
11 D. Yao, H. Yang, Q. Hu, Y. Chen, H. Chen and P. T. Williams, *Appl. Catal., B*, 2021, **280**, 119413.
12 H. Shokry, M. Elkady and E. Salama, *Sci. Rep.*, 2020, **10**, 10265.
13 M. Samy, A. G. Kumi, E. Salama, M. ElKady, K. Mensah and H. Shokry, *Process Saf. Environ. Prot.*, 2023, **169**, 337–351.
14 S. Shen, W. Jiang, Q. Zhao, L. He, Y. Ma, X. Zhou, J. Wang, L. Yang and Z. Chen, *Sci. Total Environ.*, 2023, **859**, 160001.
15 L. Li, Z. M. H. M. Shafie, T. Huang, R. Lau and C.-H. Wang, *Chem. Eng. J.*, 2023, 141342.
16 N. T. Hanh, H. An, N. T. Tinh, N. T. H. Nam, C. Q. Cong, N. D. Hai, N. M. Dat and N. H. Hieu, *Mater. Lett.*, 2023, 134591.
17 Q. Li, A. Faramarzi, S. Zhang, Y. Wang, X. Hu and M. Gholizadeh, *Energy Convers. Manage.*, 2020, **226**, 113525.

18 A. I. Osman, C. Farrell, A. H. Al-Muhtaseb, A. S. Al-Fatesh, J. Harrison and D. W. Rooney, *Environ. Sci. Eur.*, 2020, **32**, 1–12.
19 P. K. Tripathi, S. Durbach and N. J. Coville, *Appl. Sci.*, 2019, **9**, 2451.
20 M. Al-asadi and N. Miskolczi, *Energies*, 2020, **13**, 1284.
21 S. Saconsint, N. Sae-Tang, A. Srifa, W. Koo-Amornpattana, S. Assabumrungrat, C. Fukuhara and S. Ratchahat, *Sci. Rep.*, 2022, **12**, 15195.
22 S.-L. Wu, C.-M. Chen, J.-H. Kuo and M.-Y. Wey, *Chem. Eng. Sci.*, 2020, **217**, 115541.
23 W. Yang, L. Cao, W. Li, X. Du, Z. Lin and P. Zhang, *Ionics*, 2022, **28**, 3489–3500.
24 J. N. Cruz, K. D. Martínez, D. Á. Zavariz and I. P. Hernández, *J. Ecol. Eng.*, 2022, **23**, 319–330.
25 Y. Peng, Y. Wang, L. Ke, L. Dai, Q. Wu, K. Cobb, Y. Zeng, R. Zou, Y. Liu and R. Ruan, *Energy Convers. Manage.*, 2022, **254**, 115243.
26 R. Miandad, M. Rehan, M. A. Barakat, A. S. Aburiazaiza, H. Khan, I. M. Ismail, J. Dhavamani, J. Gardy, A. Hassanpour and A.-S. Nizami, *Front. Energy Res.*, 2019, **7**, 27.
27 S. Dong, J. Li, S. Zhang, N. Li, B. Li and L. Ge, *J. Polym. Res.*, 2021, **28**, 1–10.
28 R. Shoukat and M. I. Khan, *Microsyst. Technol.*, 2022, **28**, 885–901.
29 M. Kolahdouz, B. Xu, A. F. Nasiri, M. Fathollahzadeh, M. Manian, H. Aghababa, Y. Wu and H. H. Radamson, *Micromachines*, 2022, **13**, 1257.
30 M. R. Mohammad, D. S. Ahmed and M. K. Mohammed, *J. Sol-Gel Sci. Technol.*, 2019, **90**, 498–509.
31 A. Awadallah-F and S. Al-Muhtaseb, *Sci. Rep.*, 2020, **10**, 4878.
32 M. X. Tran, R. E. A. Ardhi, G. Liu, J. Y. Kim and J. K. Lee, *Chem. Eng. J.*, 2020, **401**, 126075.
33 E. Salama, M. Samy, H. Shokry, G. El-Subruiti, A. El-Sharkawy, H. Hamad and M. Elkady, *Sci. Rep.*, 2022, **12**, 22443.
34 M. F. Elkady, H. S. Hassan, W. A. Amer, E. Salama, H. Algarni and E. R. Shaaban, *Materials*, 2017, **10**, 1355.
35 A. Raoof Mahmood, M. A. Alheety, M. M. M. Asker, A. Zyaad Tareq and A. Karadağ, *J. Phys.: Conf. Ser.*, 2019, **1294**, 052003.
36 R. Al-Gaashani, A. Najjar, Y. Zakaria, S. Mansour and M. Atieh, *Ceram. Int.*, 2019, **45**, 14439–14448.
37 R. E. A. Ardhi, G. Liu, M. X. Tran, C. Hudaya, J. Y. Kim, H. Yu and J. K. Lee, *ACS Nano*, 2018, **12**, 5588–5604.
38 Z. Mehmood, M. Aamir, M. Sher, M. Sohail, R. Qadeer, N. Revaprasadu, M. A. Malik and J. Akhtar, *Optik*, 2019, **197**, 163035.
39 R. Panickar, C. Sobhan and S. Chakravorti, *Vacuum*, 2020, **172**, 109108.
40 H. S. Hassan, D. Abol-Fotouh, E. Salama and M. F. Elkady, *Sci. Rep.*, 2022, **12**, 8774.
41 E. A. Trusova, I. V. Klimenko, A. M. Afzal, A. N. Shchegolikhin and L. V. Jurina, *New J. Chem.*, 2021, **45**, 10448–10458.
42 A. M. Saad, A. Y. M. Alabdali, M. Ebaid, E. Salama, M. T. El-Saadony, S. Selim, F. A. Safhi, S. M. ALshamrani, H. Abdalla and A. H. Mahdi, *Molecules*, 2022, **27**, 5640.
43 R. E. A. Ardhi, G. Liu, J. Park and J. K. Lee, *Energy Storage Mater.*, 2023, **54**, 863–874.
44 D. Balarak, M. Zafariyan, C. A. Igwegbe, K. K. Onyechi and J. O. Ighalo, *Environ. Processes*, 2021, **8**, 869–888.
45 C. Zhang, W. Song, X. Zhang, R. Li, S. Zhao and C. Fan, *J. Mater. Sci.*, 2018, **53**, 9429–9448.
46 E. Salama, M. Ghanim, H. S. Hassan, W. A. Amer, E.-Z. M. Ebeid, A. H. El-Shazly, M. Ossman and M. F. Elkady, *RSC Adv.*, 2022, **12**, 18363–18372.
47 I. Albaik, K. E. Diab, M. Saleh, R. Al-Dadah, S. Mahmoud, M. B. Elsheniti, İ. Solmaz, E. Salama, H. S. Hassan and M. F. Elkadi, *Sustain. Energy Technol. Assess.*, 2023, **56**, 103006.
48 J. Ederer, P. Janoš, P. Ecorchard, J. Tolasz, V. Štengl, H. Beneš, M. Perchacz and O. Pop-Georgievski, *RSC Adv.*, 2017, **7**, 12464–12473.
49 E. Aliyev, V. Filiz, M. M. Khan, Y. J. Lee, C. Abetz and V. Abetz, *Nanomaterials*, 2019, **9**, 1180.
50 E. Salama, A. Hamdy, H. S. Hassan, W. A. Amer, E.-Z. M. Ebeid, M. Ossman and M. F. Elkady, *Adsorpt. Sci. Technol.*, 2022, **2022**, 6818348.
51 R. E. A. Ardhi, G. Liu and J. K. Lee, *ACS Energy Lett.*, 2021, **6**, 1432–1442.
52 F. Farivar, P. Lay Yap, R. U. Karunagaran and D. Losic, *C*, 2021, **7**, 41.
53 S. ullah Rather, *Int. J. Hydrogen Energy*, 2020, **45**, 4653–4672.
54 K. E. Diab, E. Salama, H. S. Hassan, A. A. El-moneim and M. F. Elkady, *Polymers*, 2021, **13**, 3869.
55 K. E. Diab, E. Salama, H. S. Hassan, A. El-moneim and M. F. Elkady, *Sci. Rep.*, 2021, **11**, 1–13.
56 E.-S. Duraia and A. Almaqwashi, *Ain Shams Eng. J.*, 2021, **12**, 1017–1024.